The Belvedere Glacier elevation change between 1951 and 2023

Lukáš Brodský[1,*], Shruti Pancholi[1], Susanne Schmidt[2], Marcus Nüsser[2,3], Roberto Sergio Azzoni[4], Gianluca Tronti[4]

[1] Charles University, Faculty of Science, Department of Applied Geoinformatics and Cartography, Czechia
[2] Heidelberg University, Department of Geography, South Asia Institute, Germany
[3] Heidelberg University, Heidelberg Center for the Environment, Germany
[4] University of Milan, Earth Science Department, "A. Desio", Italy
[*] Correspondence author: lukas.brodsky@natur.cuni.cz

ABSTRACT

This study describes and analyses elevation changes in the debris-covered tongue of the surge-type Belvedere Glacier (Western Italian Alps) between 1951 and 2023 using remote sensing data, including historical aerial photographs, Lidar and drone acquisitions. High-resolution digital surface models from 1951, 2009 and 2023 enabled detailed observation of the spatially heterogeneous patterns of change caused by debris cover, avalanches, a surge-type event, supraglacial meltwater, and glacial lake outburst floods in the context of global warming. In the period of 1951–2009, the mean rate of downwasting was quantified as 0.24 metres per year (14 metres in total), ranging from −83.5 to 32.2 metres. During the second observation period from 2009 to 2023, the mean downwasting rate was estimated to be 1.8 metres per year (25 metres in total), varying from −73.9 to 26.9 metres. The 2001–2002 surge-type event, meltwater streams and supraglacial lakes are considered to be the main drivers forcing elevation changes and shaping its spatial variation and surface structures. In general, the changes in the glacier have accelerated between 2009 and 2023. This paper demonstrates the high potential of differenced digital surface models with high spatial resolution to detect the processes of glacier dynamics in high detail.

1. Introduction

Glaciers are considered as important indicators of climate change since they react sensitively to climatic conditions (Lemke et al. 2007; Oerlemans et al. 2000; Jóhannesson et al. 1989). An accelerated mass loss of glaciers over recent decades can be observed in all mountain regions (Hugonnet et al. 2021; Zemp et al. 2019). As a result of glacier downwasting, englacial debris accumulates at the surface and leads to an expansion of supraglacial debris cover (Fleischer et al. 2021; Schmidt and Nüsser 2009; Thakuri et al. 2014; Azzoni et al. 2018). In addition, the extent and thickness of supraglacial debris cover also depend on debris supply from surrounding rock walls and glacial transport from the upper reaches (Kirkbride and Deline 2013). Thus, the relative debris coverage and the number of debris-covered glaciers will further increase due to ongoing glacier decrease resulting from climate change (Jouvet and Huss 2019, Racoviteanu et al. 2022). On a global scale, the relative debris coverage amounts to 4.4% of the glacierized area (excluding Greenland and Antarctica) with huge variations from less than 1% in the Canadian and Arctic Region to about 26% in the Caucasus and Middle East. In Central Europe, the percentage of debris-covered glacierized areas amounts to 10.4% (Scherler et al. 2018). The extent and thickness of debris cover influence the ablation rates. While the melting rates beneath thin debris layers (less than 3 cm) are higher than for clean ice, the ablation rates under thick layers of 1–2 m, become negligible (Hewitt 2005; Mattson et al. 1993). Supraglacial lakes and ice cliffs, which are regularly formed on debris-covered glaciers, mainly due to reduced glacier velocity and gentle slope angles in the ablation zone, can both increase ablation rates (Bhambri et al. 2023; Brun et al. 2016; Huo et al. 2021; Pellicciotti et al. 2015; Salerno et al. 2017). As a consequence, mass loss rates can be higher in the middle parts of the glacier than in the debris-covered terminus (Benn et al. 2012). In contrast, other studies from the Himalayas showed that the lowering rates of debris-covered glaciers are the same or even higher than for clean-ice glaciers (Kääb et al. 2012). Thus, the impact of debris cover on glacier mass balances is still under discussion (Hock et al. 2019; Muhammad, et al. 2020). Compared to a large number of studies on the impact of debris cover on glacier mass loss in the Himalayan region (Maurer et al. 2019), only a few debris-covered glaciers were so far investigated in the European Alps (Fleischer et al. 2021; Fugazza et al. 2023; Fyffe et al. 2019).

Debris-covered glacier surfaces are subject to extensive and rapid climate-induced geomorphological changes (Westoby et al. 2020). Several evolution patterns are described in detail: localised debris thinning across ice cliff faces, except those which were decaying, where debris thickened; pervasive debris thinning across larger, back-wasting slopes, including those bordered by supraglacial streams, as well as ingestion of debris by a newly exposed englacial conduit. These findings highlight a fast evolution of the morphology of debris-covered glacier leading to effects not only in ice melting magnitude and distribution but also inhibits across-glacier meltwater flow, both supra- and sub glacially (Mölg et al. 2020; Racoviteanu et al. 2022). Consequently, the investigation of the evolution pattern of the debris-covered glacier surface with remote-sensing data is needed (Westoby et al. 2020).

Ground measurements (Huss and Bauder 2009; Zemp et al. 2009; Fujita and Nuimara 2011; Yao et al. 2012), remote-sensing observations (Rignot et al. 2003; Bolch et al. 2012; Kääb et al. 2012; Maurer et al. 2019), and modelling studies (Radić and Hock 2006; Huss et al. 2008; Immerzeel et al. 2013) have all contributed to the documentation of volumetric glacier changes.

In recent years, geodetic methods based on remote sensing data are commonly used for estimating mass balance (Fischer et al. 2015; Kääb et al. 2012; Nuimura et al. 2017; Pellicciotti et al. 2015). Elevation changes contribute to the estimation of volume and mass changes of glaciers, as their mass loss or gain can be calculated using two digital elevation models (DEM) acquired at different times and an estimate of ice or snow density (Chandrasekharan and Ramsankaran 2023; Berthier et al. 2007; Paul et al. 2015; Bolch et al. 2008; Bolch et al. 2011; Bhambri et al. 2023; Nüsser and Schmidt 2021). This technique has been applied on elevation models derived from laser altimetry, and aerial stereo photographs, recently also on satellite optical stereo images, and radar data, but also on Unmanned Aerial Vehicle-acquired data (UAV, also known as drone). Each of them undertakes different procedures to retrieve elevation data. Laser altimetry is very precise but often has poor spatial coverage. Radar provides the best spatial coverage but can suffer from elevation errors due to the penetration of the radar signal into low-density snow and firn (Brenner et al. 2007; Berthier et al. 2016). Stereoscopic imagery frequently exhibits excellent spatial coverage, yet typically demonstrates lower temporal sampling and requires sufficient radiometric quality. UAV makes data capture of stereo images more affordable and provides the possibility to choose better contrast conditions and to decide the time intervals of multi-temporal monitoring, keeping the advantage of proximal surveys with high resolution (Haubek and Prinz 2013).

Retrieving quantitative characteristics of the glaciers requires dedicated processing workflows. Paul et al. (2015) provided a comprehensive overview of suitable algorithms for data processing and improvement of error characteristics. Glacier elevation changes from DEM differencing allow local or region-wide mass balance to be determined. They state that the spatial representativeness of elevation changes measurements and the density of the material gained or lost are the most critical assumptions for the task (Huss 2013; Paul et al. 2015). They mention that "elevation and volume change measurements are free

from related hypotheses and can therefore be independently converted to mass changes later using a density scenario of choice".

Several studies have already analysed elevation changes of the ablation zone of Belvedere Glacier using DSM differencing to analyse surface changes (Mondino 2015; Tonolo et al. 2020; Ioli et al. 2022; De Gaetani et al. 2021). However, these studies are based on stereo pairs over shorter periods, 2001–2003 (Mondino 2015), 2017–2019 (Tonolo et al. 2020), and 2015–2020 (Ioli et al. 2022). Only De Gaetani et al. (2021) applied the elevation change analysis for a longer period, between 1977 and 2019. The period since 1951 has not yet been analysed.

Our study aims to analyse elevation changes of the debris-covered Belvedere Glacier part between 1951 and 2023 and to estimate glacier volume changes over a 72-year period using historical stereo aerial images and recently acquired UAV imagery and Lidar data from 2009.

2. Study area

Belvedere Glacier (Fig. 1) is located on the east face of Monte Rosa (4634 m a.s.l.), a prominent peak in the Western Italian Alps on the border between Italy and Switzerland. It is one of the largest debris-covered glaciers of the Alps covering 4.51 km^2 (Mortara et al. 2009; Smiraglia et al. 2015). The debris-covered tongue reaches from about 2250 m a.s.l. to its lowest level at about 1800 m a.s.l., where it splits into two separate lobes. This tongue covers 1.8 km^2, with a length of 3 km and a maximum width of around 0.5 km. It is mostly elongated in a South-North direction. In 2001–2002 the glacier experienced a surge-type event (Kääb et al. 2004). The detailed study area description can be found in Kropáček et al. (2024).

3. Data sources

A combination of stereoscopic optical aerial images, UAV remote sensing imagery, and Lidar data (Geoportale Piemonte 2024) was used. Firstly, 16 grayscale analogue aerial images from 1951, were acquired from the IGM-Italian Military Geographic Institute. Secondly, 2198 digital UAV (DJI Mavic 2) images of the main ablation area and moraines from 2023, were acquired by the authors. The UAV acquisition covers only the ablation part of the Belvedere Glacier system given the limits of the UAV. Thirdly, the 5 m resolution Lidar Digital Surface Model and 0.4 m resolution orthophoto, were acquired from Geoportale Piemonte in 2024.

The quality of grayscale aerial historical images from 1951 can be characterised as generally
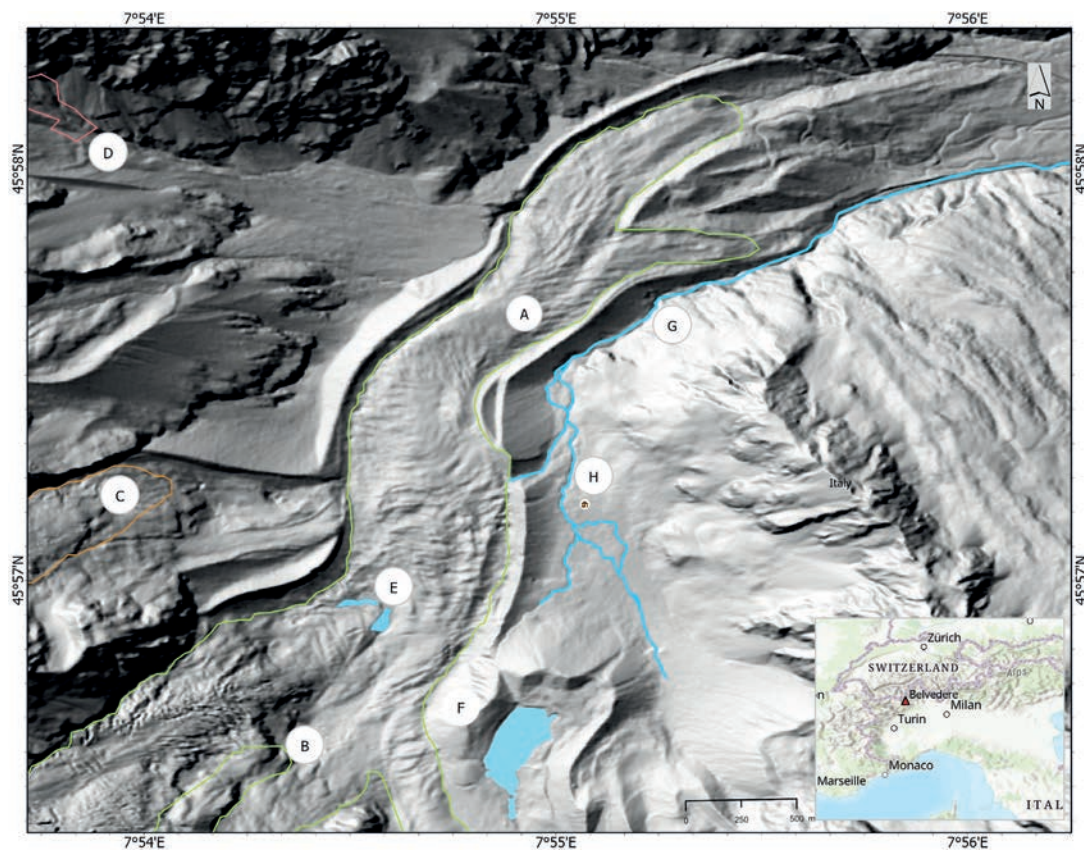
Fig. 1 A – Belvedere Glacier in green, 7°55′E, 45°57′N, B – Monte Rosa East face, C – Nordend Glacier (brown), D – Castelfranco Glacier (pink), E – Effimero Lake, F – Lago delle Locce, G – Torrent Pedriola creek, H – Zamboni-Zappa hut. Data source: DSM hillshade (Geoportale Piemonte 2024), Glacier boundaries Azzoni et al. (2024, in this issue), OpenStreetMap 2017.
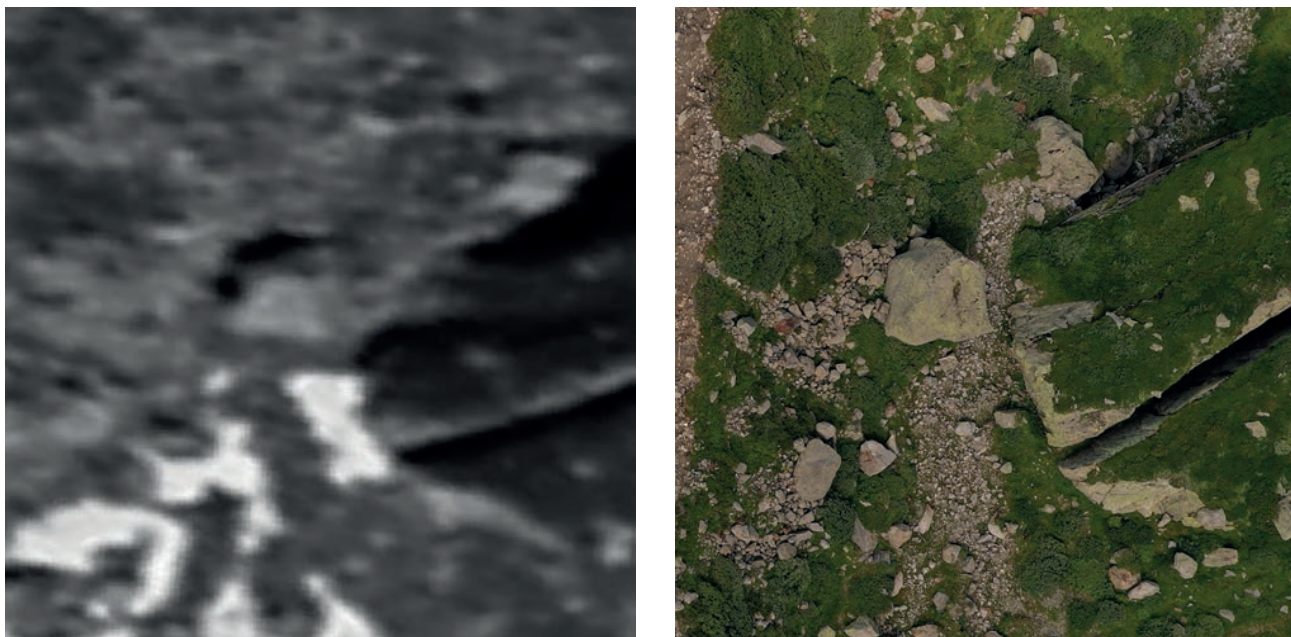
Fig. 2 Sample of historical aerial imagery in 1951 and a sample of UAV image in 2023 from the orographic-right moraine of Belvedere Glacier.

acceptable for 3D reconstruction but limited in spatial resolution (Fig. 2). The images were scanned at 10 μm/px resolution by Epson Expression 12000 XL scanner by the Istituto Geografico Militare. These cover the Belvedere main body and the two main lobes, allowing the recognition of main important features such as fractures and particular rocks on and near the moraines. The comparison between historical and modern data should consider the different spatial resolutions, such as the 3 cm resolution of UAV images. However, given the high geomorphological dynamics of the area, and the corresponding displacements of features, this comparison is possible.

The 2023 consecutive strips of digital RGB images acquired by UAV (Fig. 3) are well distributed over the debris-covered Belvedere Glacier and moraines with 70% frontal as well as side overlap. The survey was mainly concentrated on the glacier part with the ephemeral lake. It was not possible to cover the entire western moraine area due to the large size and the weather conditions during the surveys.

Tab. 1 Cameras characteristics.

Date	Aircraft	Camera	Sensor	Focal length (mm)	Image size (px)
1951/08/24	N/A	Santoni	Analog, (glass 13 × 18)	195	~12800 × 17700
2023/08/02	DJI Mavic 2	Hasselblad	RGB CMOS 1/2.3″	28	4000 × 3000

DSM realised through airborne Lidar surveys 2009, 5-metre spatial resolution, is considered as a reference model in this study. The associated 0.4-meter resolution orthophoto was received from the same survey.

Fig. 3 Sample of raw UAV images with an overlap of 70% (Date: 2023/08/02).

4. Methods

The process of analysing the volume changes from the multi-temporal dataset began with the processing of historical stereo images to generate a DSM for change detection.

4.1 Ground Control Points collection

The ground control points (GCP) and control points (CP) were used for the purposes of referencing and correcting the models and orthophotos. A total of 24 GCPs and CPs were used for the historical orthophotos from 1951, while 26 GCPs and CPs were employed for the 2023 surveys.

The GCPs (and CPs) for the 1951 image processing were partly (13) measured in-situ on natural features and partly (11) identified on the 0.4 m orthophoto.

The in-situ measured GCPs were collected using Trimble R12i GNSS System with differential signal from RTX. Notable and recognisable flat features, such as large rocks, were selected. The coordinates and elevations of these GCPs were collected in-situ with the associated accuracy, the initial threshold accuracy for the coordinates collection was set to 0.1 m. These natural GCPs are marked with the starting letter "N" and a number in Fig. 4. The additional 21 GSPs identified on the 0.4 m orthophoto used the original Lidar Digital Surface Model received from Geoportale Piemonte in 2024.

The GCPs (and CPs) for the 2023 image processing were partly (16) measured in-situ (Trimble R12i GNSS System) on natural features and partly (10) provided by the Politecnico di Milano (De Gaetani et al. 2021; Ioli et al. 2022). There were 27 50 × 50 cm polypropylene markers identified as fixed points on the stable deposits and measured with a high-quality Global Navigation Satellite System (GNSS). Field measurements were made using a dual-frequency (L1/L2) geodetic quality GNSS receiver Leica GS14 (De Gaetani et al. 2021). In the upper part of the glacier, a real-time kinematic RTK correction was applied (~10 min time sampling, 1 Hz sampling rate). For the rest of the markers, a post-processing approach was adopted using a local master station (Leica GPS1200). The official European reference system ETRF2000 was used, resulting in a coordinate accuracy of 1.5 cm in planimetry and 3 cm in elevation, in terms of root mean square error (RMSE) (De Gaetani et al. 2021). However, only seven of the high-quality GCPs could be utilised for the 2023 data processing (Fig. 4, marks starting with "D"), and three CPs allocated for validation purposes. The high-quality points only covered the lower part of the glacier.

4.2 Historical aerial stereo image processing

The 16 grayscale aerial photographs from 1951 were processed to generate DSM surfaces for reconstructing morphometric changes. The generation of stereo models was performed with the SfM

(Structure-from-Motion) Agisoft Metashape Professional v. 1.7.5 (Agisoft 2024). The inner and outer orientations of the scanned images were calibrated by Agisoft to obtain a stereo model. Manual camera protocol or camera orientation parameters were not applied before the SfM process as they were not available.

The tie points were automatically generated for the orientation of the scenes by the software.

To acquire the six parameters of interior and exterior orientation, a bundle block adjustment method was used in Agisoft. 15 GCPs and 9 CPs were utilised for the bundle block adjustment process. A measured accuracy of the natural GCPs were utilized for reference weighting. Taking into account the data density, the final DSM grids were generated with a ground resolution of 0.1 m. The root mean square error (RMSE) was used as evaluation metrics:

$$RMSE = \sqrt{\frac{\sum_{i=1}^{n}(x_i - y_i)^2}{n}},$$

where x_i and y_i are the coordinates of the GCPs or CPs, and n is the number of points.

4.3 UAV stereo image processing

The workflow for UAV stereo image processing follows in principle the process as presented in chapter 4.1. The model generation was performed with the SfM running the same software.

The UAV flight elevation was fixed at 100 m above ground level from the starting point, providing a theoretical ground sampling distance of 3.2 cm. The mission planner Pix4Dcapture v.4.11.0 (Pix4D 2024) was used to parametrize the image capture in a single grid, a camera angle 90°. In total, 2198 images were acquired over the main part of the debris-covered glacier and side moraines.

26 targets spread along the glacier were used as CPs and selected in each image, 17 GCPs for the alignment process and 9 CPs for the error estimation. The accuracy of the individual GCP markers was set based on the in-situ measurements using the Trimble R12i instrument and 0.03 m for the Politecnico di Milano GCPs.

The 3D reconstruction starts with the automatic recognition of Tie and Key points through *Scale Invariant Feature Transform-SIFT* algorithms and the alignment process through *SfM* algorithms, obtaining the *Sparse Cloud* and the Camera orientation.

The 3D reconstruction process continues through Multi-View Stereo algorithms, applied to obtain the *Dense Cloud.* The last phase consists of the DSM generation, using the depth maps generated through the previous process, obtaining a 0.1 m raster DSM.

4.4 Change analysis

The change analysis involves comparing two or more DSMs acquired at different time points to identify and

quantify changes in the terrain's elevation. The measurement of changes in glacier elevation by differencing is a widely used method for estimating changes in glacier volume and mass at local and regional scales (Sommer et al. 2020; Bhambri et al. 2023).

Before making a relative DSM comparison, it was assured that the DSMs from different time points are co-registered. This step is critical for accurate differencing. The datasets were resampled to the common 1 m spatial resolution prior to the co-registration as a compromise between the 0.5 m resolution from the historical and UAV data processing and the 5 m resolution from the 2009 elevation model.

The co-registration procedure is based on the method proposed by Knuth et al. (2023). They introduced a multi-stage co-registration method, which involved a point cloud alignment method followed by the slope and aspect dependent method by Nuut and Kääb (2011). An iterative co-registration approach is used, which means that the co-registration process is performed in several iterations to progressively refine the alignment. The point clouds of the terrain models for the years 1951 and 2023 were finely co-registered with the 2009 Lidar point cloud (Geoportale Piemonte 2024) as the reference. The point

pair picking alignment tool of CloudCompare software was used for this process. Specific masking (glacier boundaries: Azzoni et al. 2024, in this issue) was used to perform co-registration outside the glacier. The co-registration process involves minimising the sum of squares of the distances between corresponding points in the DSMs. This is a common optimization approach to achieve the best alignment. The outputs are aligned DSMs and the co-registration parameters, which refer to the transformation parameters applied to one or more DSMs to align them with the reference.

The quantified elevation change of the glacier is the input information for the following step, the estimation of the volume of ice gained and lost. An estimation of the changes in glacier elevation across two intervals is performed, using a well-established process called DSM differencing. The two differenced DSMs enable to estimate the volume changes between 1951 and 2023. They are used to estimate the spatial variation of volume changes corresponding to the mean, minimum, and maximum differences for the periods 1951–2009, 2009–2023, and 1951–2023. The volume change is calculated over a constant area of the glacier and surrounding region. The UAV-derived DSM in 2023 was used to delineate the glacier boundary. The DSMs (1951 and 2009) were clipped by the extent of the 2023 DSM and later by the glacier boundary shapefile. The study area is approximately 1.6×10^6 m^2 in size. To calculate the mass change of the Belvedere Glacier, the density of ice was assumed to be 850 ± 60 kg m^{-3} following Huss (2013).

5. Results

The combination of GNSS measurements and manually selected GCPs allowed the generation of high-resolution DSMs of the complex terrain of Belvedere Glacier ablation area and its orthophotos (Tab. 2, Fig. 5). The accuracy of the 1951 DSM in the vertical dimension amounts to −0.68 m on CPs. Some problems in the 1951 DSM can be detected in the southern part of the glacier, where visible outliers create high-frequency texture patterns. They are also partially visible in the northern terminus of the main tongue. This area also suffers from some erratic points, and local errors in the 1951 DSM due to imprecise image matching and low image quality, but these artefacts do not affect the main trends in the topographic changes analysed in this study. The UAV-derived DSM 2023 resulted in a much higher accuracy of −0.08 m compared to the historical 1951 DSM processing (Tab. 2). The precision of the natural GCPs, determined through the utilisation of the Trimble R12i GNSS with RTX differential data enhancement, exhibited a mean value of 0.017 m in Easting, 0.094 m in Northing, and 0.045 m in elevation.

Fig. 5 illustrates the DSM related orthophotos as part of the photogrammetric process. The 1951
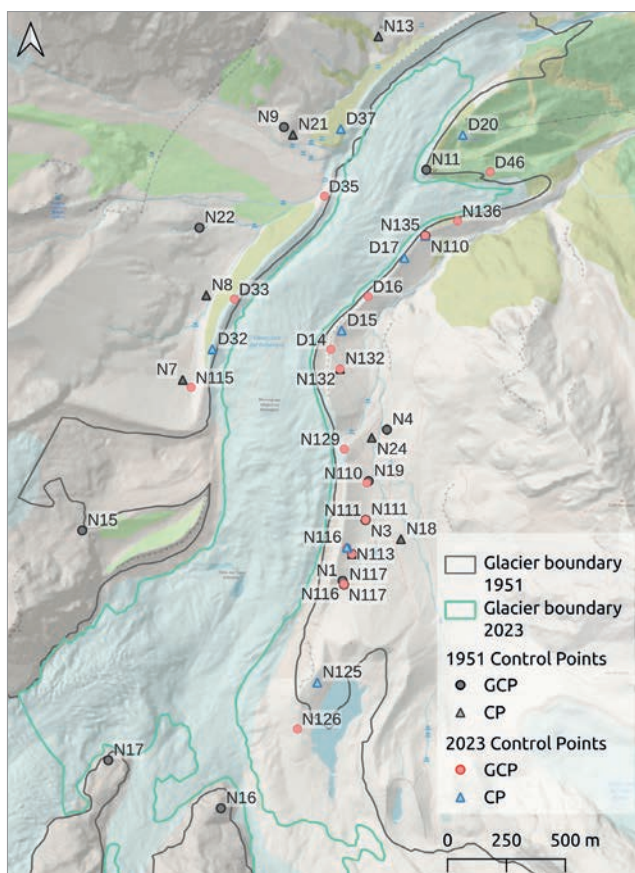
Fig. 4 Location of the Control Points used for the photogrammetric models, background: OpenStreetMap data (OpenStreetMap 2017) and the 2009 hill-shade derived from Lidar DSM 2009 (Geoportale Piemonte 2024)
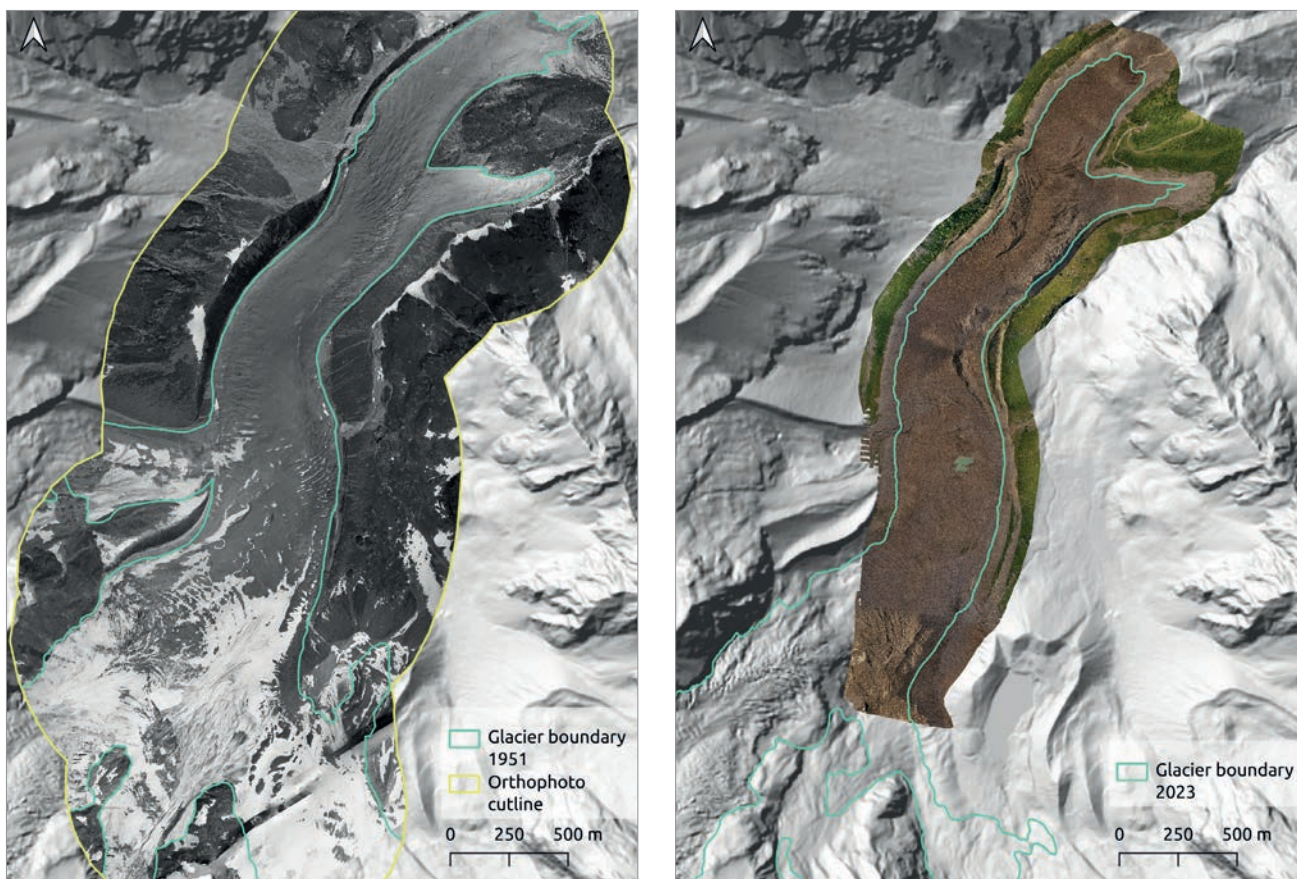
Fig. 5 Belvedere Glacier orthophotos from aerial 1951 and UAV 2023 images and hill-shade derived from Lidar DSM 2009 (Geoportale Piemonte 2024).

Tab. 2 RMSE computed on CPs for each photogrammetric model.

DSM	E (m)	N (m)	h (m)
1951	−0.25	−0.04	−0.68
2023	0.39	0.06	−0.08

E, N, h – ground coordinates Easting, Northing, and elevation

grayscale orthophoto appears compact over the entire area of the glacier and its surroundings, although there are some irregular outliers. The 2023 orthophoto (Fig. 5, right) shows a number of cloud shadows (radiometric variability) along the debris-covered glacier. The changing weather conditions partly affected the accuracy of the image matching, which propagated into the DSM quality.

Although the accuracy of the retrieved 1951 and 2023 DSMs is relatively high, the aim was to compare the independently processed models. The

comparison preceded the co-registration process. The accuracy assessment of the relative DSMs after co-registration is presented in Tab. 3. It presents an evaluation of how well the DSMs align with a common reference model 2009. The Tab. 3 shows key parameters after the co-registration, the mean values are well near zero, however, the spread of the points reveals variations.

Tab. 3 DSM post-co-registration statistics.

DSM compared to 2009 reference	Mean (m)	Median (m)	RMSE (m)
1951	0.386	−0.051	0.91
2023	−0.394	0.0712	0.71

Note: the glacier was masked a priory of the co-registration process with outliers defined as mean ± 3 sigma of the DSM differences outside of glacier.

Tab. 4 Elevation and volume changes of the Belvedere Glacier tongue (excluding the Monte Rosa east face).

	Mean Elevation Change	Total Volume Change [m³ × 10⁶]	Volume Change [m³ × 10⁶ yr⁻¹]	Mass Change [Mt]	Mass/unit area [kg/m²]	Mass balance [m w.e.]	Annual mass change [m w.e. yr⁻¹]
1951–2009	−14.01	−15.73	−0.27	−13.37 ± 0.27	−11899.41	−11.89	−0.21
2009–2023	−24.82	−27.95	−1.99	−23.71 ± 1.67	−21105.92	−21.14	−1.51
1951–2023	−38.34	−43.61	−0.61	−37.07 ± 2.61	−33002.22	−33.01	−0.46
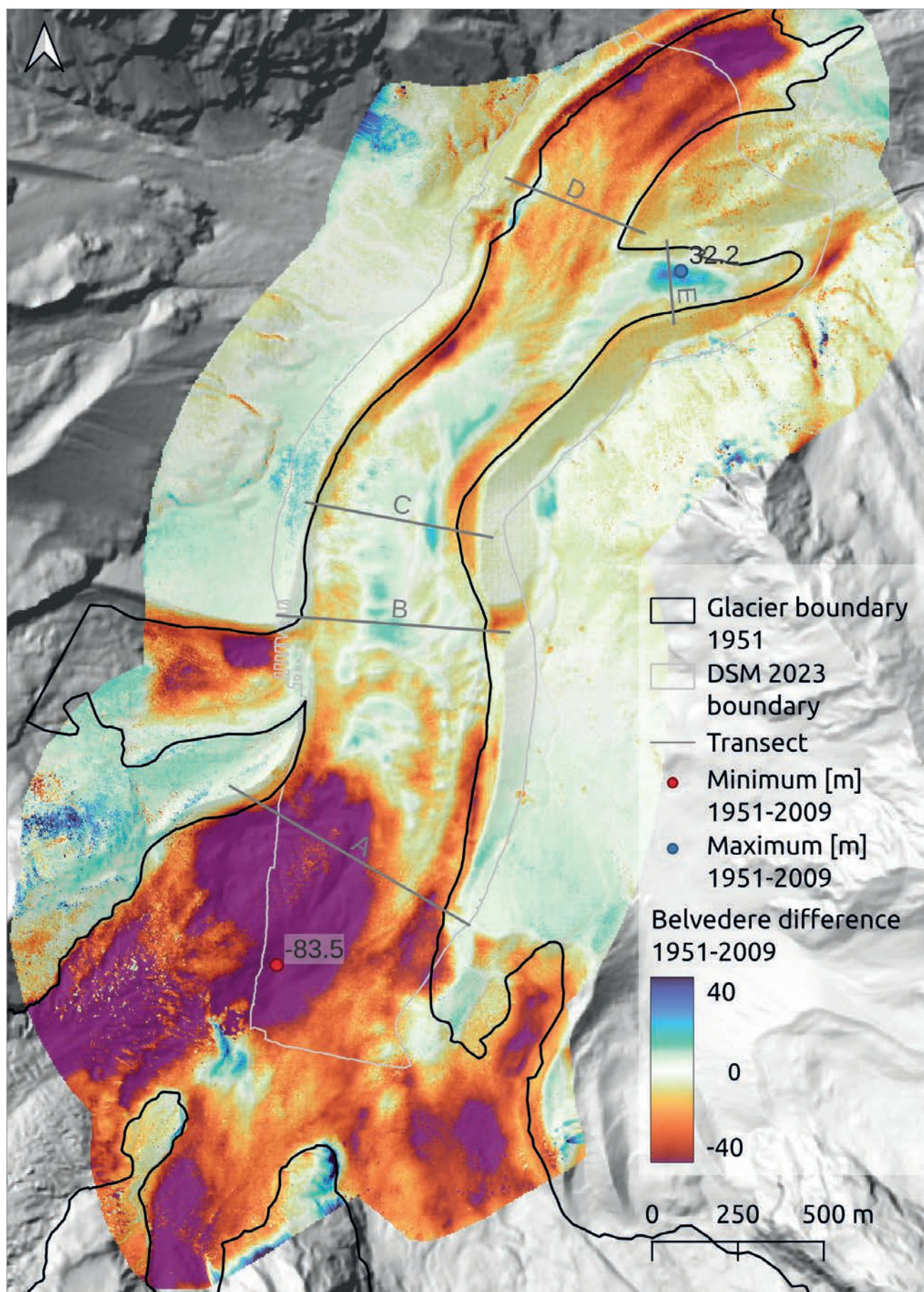
Fig. 6 Glacier elevation change between 1951 and 2009 illustrated with dichromatic colour ramp centred around 0, glacier outlines 1951 (Azzoni et al. 2024, in this issue).
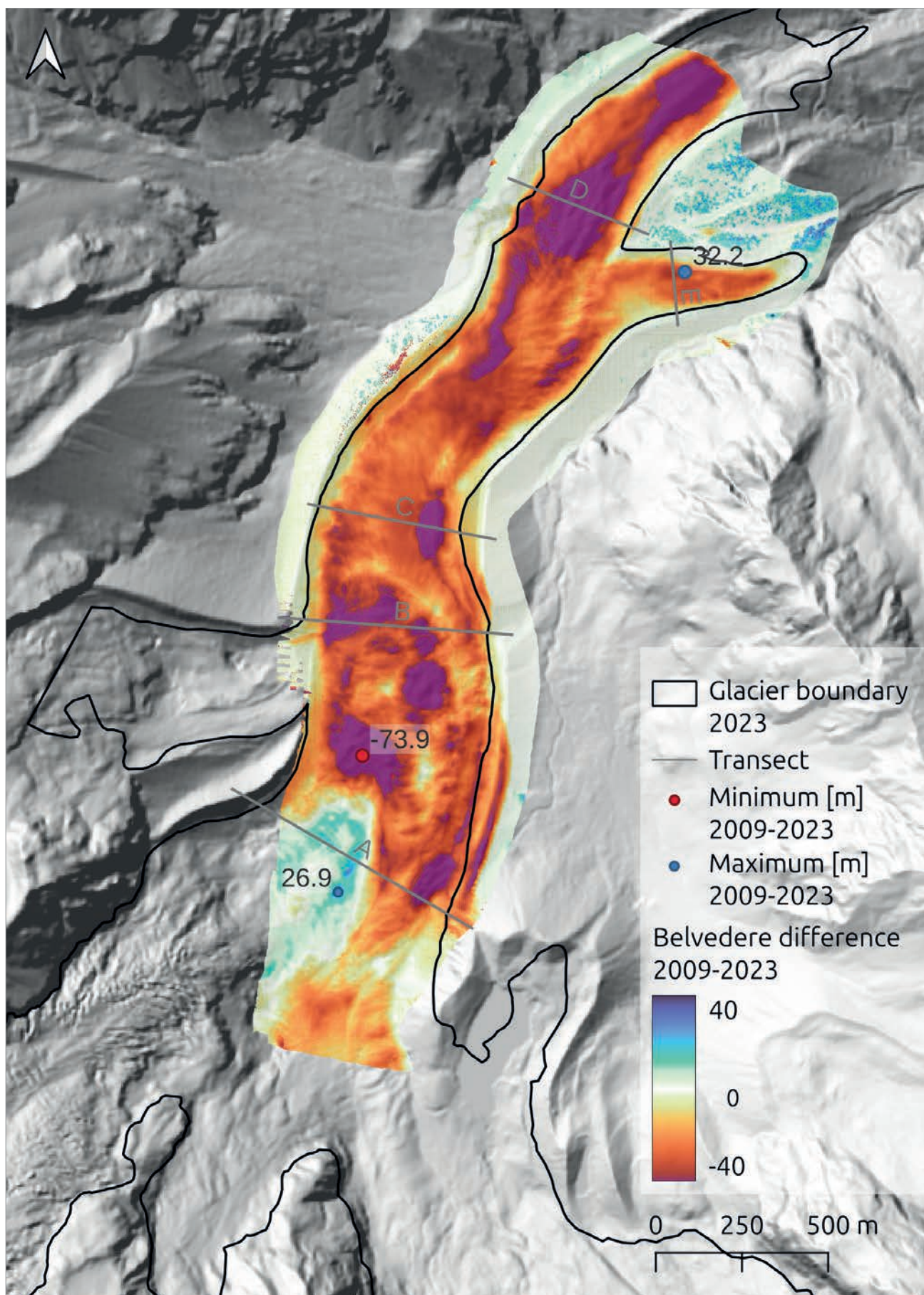
Fig. 7 Glacier elevation change between 2009 and 2023 illustrated with dichromatic colour ramp centred around 0, glacier limit 2023 (Azzoni et al 2024, in this issue).
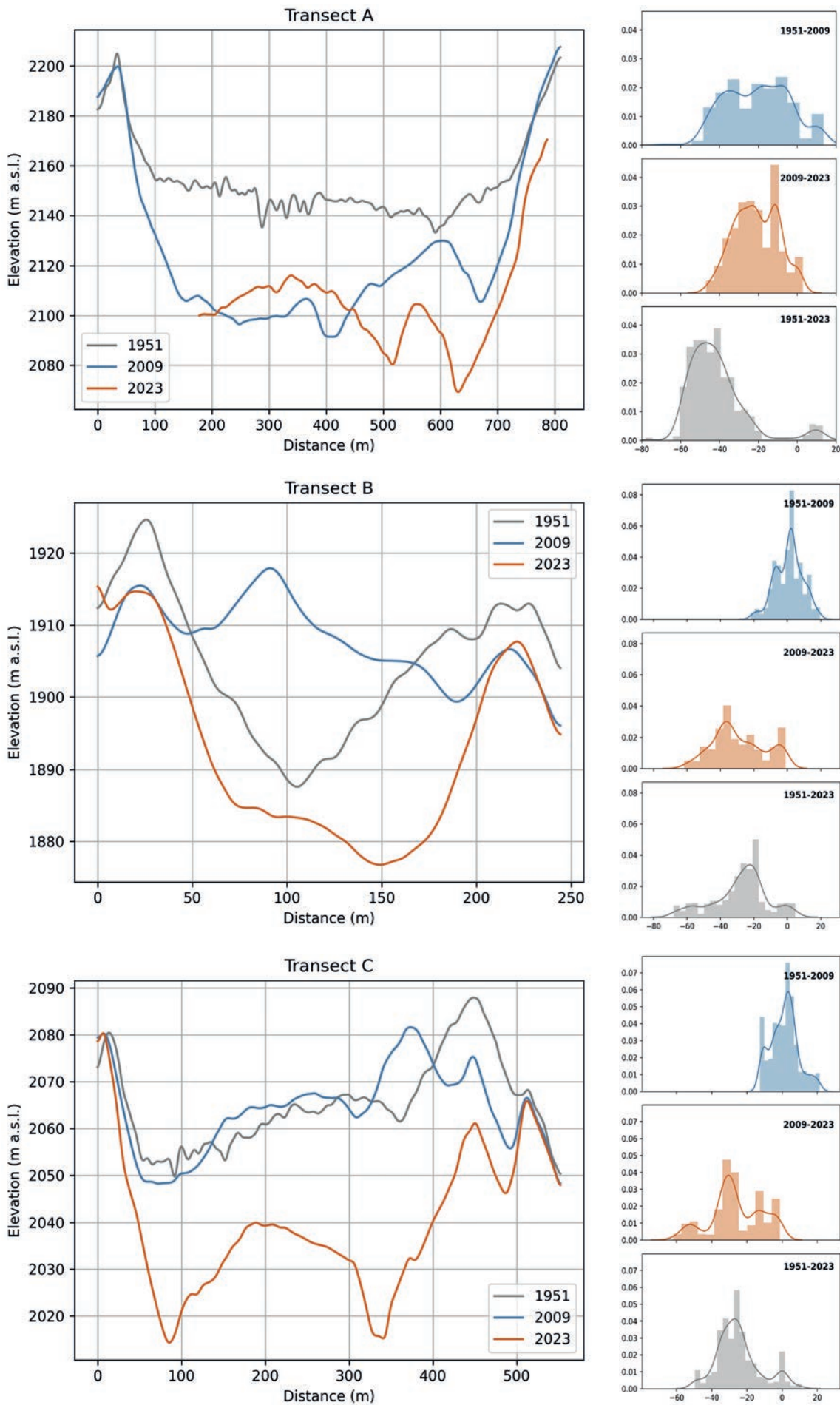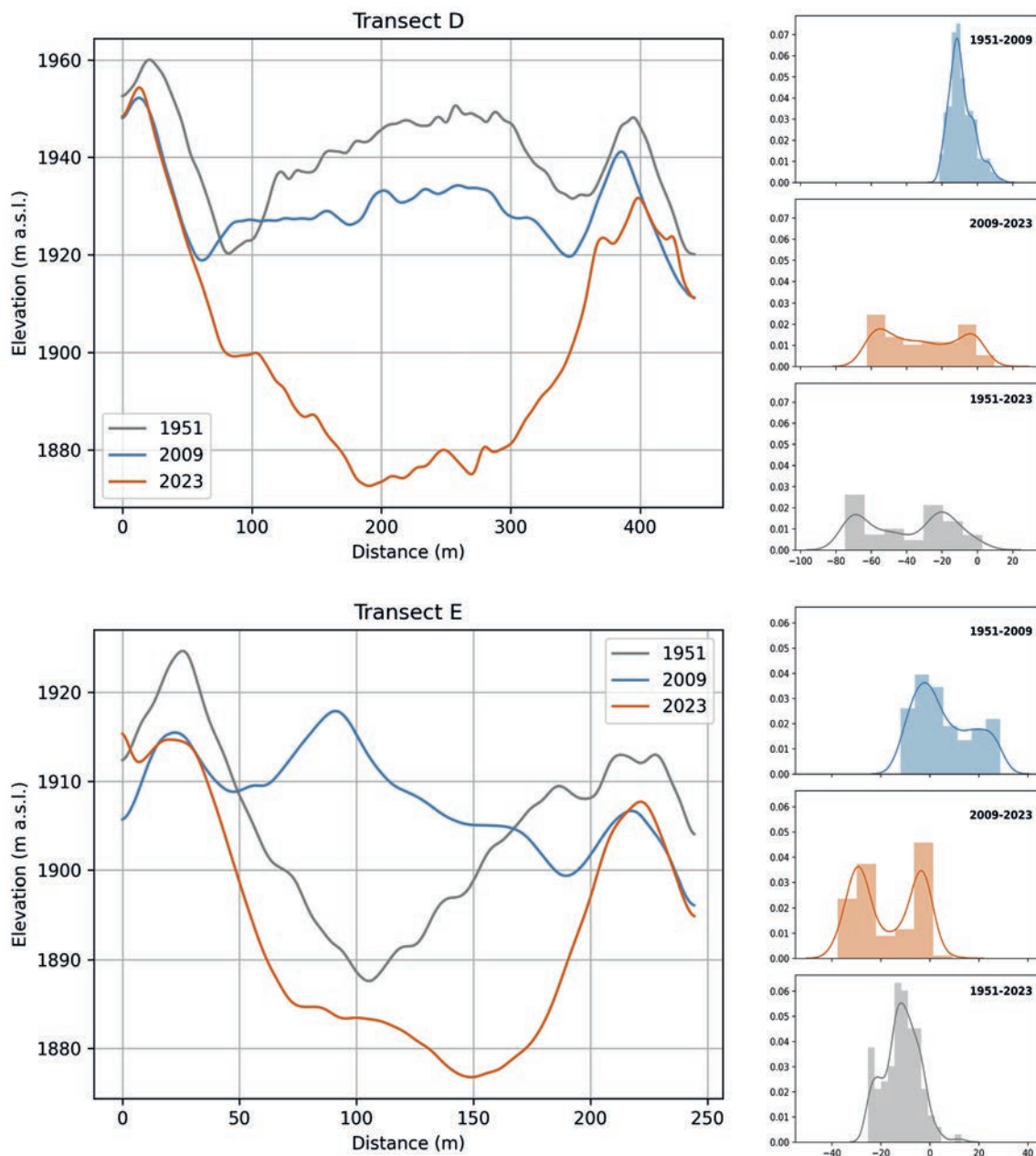
Fig. 8 Five transect profiles of the Belvedere Glacier (Fig. 6 and Fig. 7) illustrate the surface in 1951, 2009, and 2023 and the elevation changes. Transect A: transition area receiving avalanches from the Monte Rosa east face; Transect B: central part of the debris-covered glacier near the glacio-fluvial stream of Nordend Glacier and the moraine breach. Transect C: central part of Belvedere Glacier with the double moraine formation on the eastern and two water channels on both sides of the glacier. Transects D and E: the two lobes of the glacier tongue.

The differenced DSMs 1951–2009 and 1951–2023 show some changes in the vicinity of the glacier, in particular tree growth close to the terminal moraine. Other changes in the stable ground are caused by noise, which is often unavoidable when processing historical data.

Based on the differenced DSMs, significant elevation changes of the Belvedere Glacier were detected over the entire observation period 1951–2023, which amounted to a mean elevation change of −38.3 m (−0.53 m yr^{-1}) (Tab. 4). The average downwasting amounted to −0.24 m yr^{-1} between 1951 and 2009 (−14.0 m in total) , equating to a specific mass change

rate of −0.2 m w.e. yr^{-1}. In the second observation period 2009–2023, the ice loss was more than seven-fold higher at −1.77 m yr^{-1} (−24.8 m in total), equating to −1.51 m w.e. yr^{-1}. The increasing trend in the annual mean temperature is also documented in the supplement (Appendix 1). These downwasting rates of the glacier tongue (excluding the Monte Rosa east face) are equivalent to a mass loss of 13.4 ± 0.27 Mt (Megatones) from 1951–2009 and a further loss of 23.7 ± 1.67 Mt in the period 2009–2023.

In addition to the acceleration of the glacier thinning rates, large differences in the spatial pattern of elevation changes become apparent between the two

Fig. 9 Terrestrial photographs of Belvedere Glacier with distinctive geomorphological features; A: Monte Rosa east face and transition zone of Belvedere Glacier (2021/08/11); B: debris-covered tongue modulated by meltwater streams and ice-marginal channels (2023/09/30); C: drainage pipe of Lago delle Locce and collapse of the moraine (2023/09/30); D: double moraine from the North with Monte Rosa east face at background (2023/08/02); E: ice cliffs and meltwater stream from Castelfranco Glacier on the Belvedere Glacier (2022/08/09); F: Glacier terminus of the debris-covered primary lobe (2021/08/12).

observation periods (Fig. 6–8, Transect A-D). Along the central part of the glacier tongue, the surface lowering amounted to less than −10 m (Fig. 8, Transect B and Transect C) with some small parts with mass gain. The highest mass gain of up to 32.2 m can be identified at the secondary lobe, despite the fact that the frontal position of the glacier retreated by about 70 m (Fig. 8, Transect E). Some spots with a much higher surface lowering can be identified along the glacier tongue with a maximum of 83.5 m in the transition zone at the foot of Monte Rosa east face. In this part, the depression of the Effimero Lake was formed in 2002 and completely drained in 2003 (Transect A). Furthermore, the retreat of the primary lobe (Transect D) by about 170 m (Azzoni et al. 2024, in this issue) and of the Nordend Glacier by about 755 m (in the timeframe 1951–2021 since the UAV orthophoto is not available for this area) become evident by high mass losses.

In contrast to the first period, the entire glacier tongue is characterised by massive downwasting during the second observation period 2009–2023. Thus, in all transects the glacier surface is lower than in 1953. Some areas of more pronounced downwasting up to −73.9 m can be identified (Fig. 6), which appear as a series of depressions distributed along the entire glacier tongue. Some of these depressions are at least temporarily filled with water (Fig. 7) and one of them (Fig. 8, Transect B) is connected to the glacio-fluvial stream of Nordend Glacier, flowing to the Belvedere Glacier and visible as a small line in the differenced DSM. Furthermore, along the eastern margin of the tongue, two linear structures with accelerated mass loss are visible, connected to the outlet of Lago delle Locce. Compared to the former period, both glacier lobes showed drastic downwasting with a decrease of about −70 m and −25 m at the primary and secondary lobe, respectively. In addition to the thinning of the glacier, the collapse of the lateral moraine becomes visible as a characteristic double structure in the differenced DSMs (Fig. 8, Transect C). Only in the southern part of the tongue, the transition zone to the Monte Rosa east face (Transect A), a maximum increase of 26.9 m can be observed (Fig. 7).

In addition to the accelerated thinning of the glacier, there are also notable changes in certain geomorphological features (Fig. 6–8), such as the widespread collapse of lateral moraines amounting up to 40 m due to debuttressing and the breach (width 80 m) in the eastern lateral moraine caused by the surge-type event in 2001–2002 as well as downwasting (up to 60 m) due to meltwater from the tributary Castelfranco Glacier and from Lake Locce (up to 55 m). Furthermore, the formation of a double-crested moraine is dislocated by up 60 m on the eastern lateral moraine and is highlighted in Profile C of Fig. 8. Moreover, the moraine in the vicinity of Lake Locce decreased by about 40 m, as indicated by transect A.

6. Discussion

The multitemporal change analysis of Belvedere Glacier provides valuable insights into the dynamics over the period 1951–2023. The combination of historical, UAV, and aerial data, along with the DSM difference approach, contributes to a comprehensive understanding of recent changes of debris-covered glaciers in the region.

6.1 Elevation data

The DSM from 1951 has been processed for the first time. Although there are some visible outliers (probably caused by mass movements and vegetation growth), the digitization of the historical data allowed the creation of a digital representation of the historical glacier surface with a high spatial resolution, enabling the detection of long-term elevation changes. The accuracy of the retrieved DSM from 1951 is comparable to the accuracy of the DSM from 1977 processed by De Gaetani et al. (2021), except in the vertical dimension (RMSE 0.43 m compared to 0.91 m).

The accuracy of the 2023 DSM is comparable to UAV data processing 2020 by Ioli et al. (2022) in the upper part of the Belvedere Glacier. However, they also achieved accuracies below 0.1 m RMSE in other years.

6.2 Glacier elevation changes

The analysis of the two differenced high spatial resolution DSMs enables the detection of the complex processes and related changes of the surge-type and debris-covered Belvedere Glacier since 1951. The Belvedere Glacier belongs to the few glaciers in the Alps with positive mass balances during the second half of the 20th century. According to Diolaiuti et al. (2003), the glacier tongue has already retreated in the early 1990s, while De Gaetani et al. (2021) observed ice volume gains until the 1990s. Due to the duration of the first observation period lasting from 1951 to 2009, the period of mass gain and the reverse trend is not captured by the differenced DSMs used in the present study. However, the long observation period indicates a massive mass loss, as the glacier surface in 2023 is on average 38 m below that of 1951 (mean annual thinning rate −0.5 m per year), which is in line with the increasing trend of mean annual temperature trend since 1987, Appendix 1, statistically confirmed by Mann-Kendall test with p-value of 5.75×10^{-14}. During 2009–2023 an elevation thinning with 1.7 m per year can be observed (mass change rate of −1.5 m w.e. per year), that is much higher than for the Italian Alps, which amounted to −0.5 m per year (mass change rate of 0.6 m w.e. per year) during 2000–2014 (Sommer et al. 2020; Hugonnet et al. 2021). This comparatively high thinning rate might be caused by the exclusion of the headwall,

which forms the accumulation zone of the Belvedere Glacier. The present study examined glacier elevation changes of the debris-covered ablation zone using reference Lidar elevation points (2009) and very high-resolution images (2023 UAV ground sampling distance 3.2 cm), which resulted in elevation models with sub-meter accuracy. It can be assumed that the discrepancy between the studies can be attributed to the fact that the accumulation area was not examined in the present study. Until now, no other study has yet processed elevation changes in very high spatial resolution with sub-meter accuracy for the entire Belvedere Glacier.

It can also be assumed that the surge-type event 2001–2002 (Kääb et al. 2004) has a long-term impact on mass balances. Like in the case of the Vernagt-ferner, one of the few surge-type glaciers in the Alps showing higher mass losses after surging events (Charalampidis et al. 2018). In contrast, on the regional scale no significant differences of mass losses were observed between surge-type and non-surge glaciers in the Karakoram (Farinotti et al. 2020; Gardelle et al. 2013). However, it becomes obvious from the differenced DSM 2009–2023, that the surge-induced surface thickening of about 30 m in the upper part of the glacier tongue (from near Locce Lake to Rifugio Zamboni) (Truffer et al. 2021), completely melted. The surge movement, which probably originated from the foot of the Monte Rosa east face (Kääb et al. 2004; Truffer et al. 2021) is detectable in the differenced DSM 1953–2009 as the large depression in the transition zone near the temporary Effime-ro Lake, which bursted in June 2003 (Truffer et al. 2021). According to Kääb et al. (2004), the ice loss amounted to 20 m at this spot during 1995–1999 and a further ice loss occurred due to the surge movement. During 2009–2023, the lower part of the head-wall shows positive elevation changes, which might be a response to the rapid ice loss in the vicinity of Effimero Lake or due to the accumulation of large avalanches in 2005 and 2010, quantified by Fischer et al. (2013) and Tamburini et al. (2013). Due to the steep headwall of the Monte Rosa east face, the transition zone is characterised by frequent ice avalanches, similar to the case of the Karakoram and Nanga Parbat glaciers (Hewitt 2014; Bhambri et al. 2017; Nüsser and Schmidt 2021).

Due to the high spatial resolution of the differenced DSMs, also the accelerated ablation along water bodies can be detected. The linear features of accelerated ablation indicate ice-marginal channels and meltwater streams, such as those from the Nordend Glacier and Locce Lake and from the Castelfranco Glacier, which flow partly on the Belvedere Glacier. These streams are often connected to large depressions, some of them were formed by supraglacial lakes (Brodský et al. 2024, in this issue), others by roof collapses of englacial water bodies (Gulley and Benn 1997). To which degree this can also be related to the subglacial outburst of Effimero lake (Truffer et al. 2021) remains an open question.

Furthermore, the impact of ice cliffs, which are often connected to supraglacial lakes and increase mass loss (Bhambri et al. 2023; Brun et al. 2016; Pelliciotti et al. 2015; Salerno et al. 2017), needs to be analysed in more detail. Especially, as the typical inversion of the ablation gradient along debris-covered glaciers as shown for the debris-covered glaciers in the Khumbu region, Himalaya (Benn et al. 2012) does not exist. In contrast, the lowermost part and the transition zone of the Belvedere Glacier both showed a more pronounced thinning than the central part. The higher ablation rates along the left lobe might be caused by ice-cliffs or by a changed flow direction as it seems that the surge event fed only the smaller right lobe. As the right lobe is characterised by a thick supraglacial debris-cover, the ice loss is less pronounced compared to the left lobe. However, velocity measurements, which were carried out by Ioli et al. (2022) since 2015, showed that both lobes probably consist of stagnant ice. In the upper part, the high ablation rates might be caused by the occurrence of supraglacial lakes as well as the more patchy debris coverage.

As in other studies (De Gaetani et al. 2021; Dioliau-ti et al. 2003), the Monte Rosa east face was excluded from the calculations of changes. However, headwalls of ice and avalanche-fed debris-covered glaciers are important for an improved understanding of mass balances (Hewitt 2014; Nüsser and Schmidt 2021), often neglected in long-term models (Laha et al. 2017). Furthermore, they are important sources for the debris supply to the glaciers (Racoviteanu et al. 2022). Especially in the case of the Belvedere Glacier this is of utmost importance, where an increase of the debris-covered area can be observed since the end of the 19th century (Kropáček et al. 2024, in this issue) as Monte Rosa east face slope failures started in 1990, while several large rock and ice avalanches occurred in the 2000s (Fischer et al. 2013). The mass loss at the Monte Rosa east face was quantified, while its impact on the Belvedere Glacier is unknown.

6.3 Consequences on glacier geomorphology

In addition to the glacier changes, the differenced DSM also highlights some geomorphological changes occurred in surrounding areas. The formation of a breach in the lateral moraine caused by the surge event in 2001–2002 becomes evident with a strong erosion of the outer side of the moraine and the accumulation of the eroded material further downstream. A similar breach is evident at the base of the debris flow cone of the Castelfranco Glacier. Here, during more intense rainfall events, the debris flow channel cuts through the moraine reaching the glacier.

This action leads to a progressive enlargement of the moraine.

The significant reduction in ice thickness has led to widespread slipping of the inner margin of the moraines due to debuttressing phenomena (Azzoni et al. 2023). This is particularly evident on the left bank upstream of the breccia caused by the melting water of Castelfranco Glacier, on the left bank just downstream of Lago delle Locce (Fig. 6) and on the right side of the main lobe. Here, although the main ridge of the moraine is stable, the large loss of thickness has led to the formation of double-crested moraine as highlighted also in the profiles of Fig. 7. The displacement rate of this sliding, calculated with dendro-geomorphological analysis, is 1.87 metres per year for the 2018–2023 timeframe (Bollati et al. 2024, in this issue).

From the comparison of the DSMs, an evolution of the Belvedere Glacier moraine near Lago delle Locce is also observable. Here, also an anthropogenic impact on the geomorphology of the area is evident. In fact, following the erosion of this sector of the moraine and the alarm for a possible sudden draining of the lake, in 1979 a series of interventions were carried out that altered the shape of the moraine. Excavating a deep trench in the moraine and installing a drainage pipe diverting water to the inner side of the moraine led to significant changes in this area. The effect of this operation is still ongoing as the discharge of water pipe on the moraine's flank promotes localised erosion.

7. Conclusion and outlook

The processing of the 1951 historical data into a DSM for the first time is an important step in understanding the dynamic processes that have taken place on Belvedere Glacier over the last 72 years. The high spatial resolution of the DSMs allows detailed observation and deciphering of the spatially heterogeneous downwash pattern caused by complex processes such as debris cover, avalanches, surge, supraglacial meltwater and GLOFs, and their relationship to global warming. These high spatial resolution data are necessary for a better understanding of the response of glaciers to global warming. Downwasting of Belvedere Glacier has accelerated, as documented by the massive elevation changes between our latest observation period (2009–2023). The massive mass loss in the long term observation period is in line with the increasing trend of mean annual temperature since 1987, also statistically confirmed. While our data does not directly identify the surge-type event, the impacts are unmistakable when examined in the context of the analysed data sets. The 2001–2002 surge event, meltwater streams and supraglacial lakes are considered to be the main drivers forcing elevation changes and shaping its spatial variation and surface structures.

The compared DSMs also reveal geomorphological changes, including breaches in lateral moraines caused by glacier surges and debris flows, leading to erosion and downstream material accumulation, with similar processes observed at the Castelfranco Glacier during heavy rainfall. Also, the significant reduction in ice thickness caused widespread moraine slipping due to debuttressing, particularly near Castelfranco Glacier and Lago delle Locce.

For future work, it will be beneficial to increase the temporal resolution of DSMs to analyse glacier dynamics and associated geohazards in more detail. The area to be analysed shall include the Monte Rosa east face as well.

References

Agisoft Metashape. (2024). Available online: https://www.agisoft.com (accessed on 25 January 2024).

Azzoni, R. S., Fugazza, D., Zerboni, A., Senese, A., D'Agata, C., Maragno, D., Carzaniga, A., Cernuschi, M., Diolaiuti, G. A. (2018): Evaluating high-resolution remote sensing data for reconstructing the recent evolution of supra glacial debris: A study in the Central Alps (Stelvio Park, Italy). Progress in Physical Geography: Earth and Environment 42(1), 3–23, https://doi.org/10.1177/0309133317749434.

Azzoni, R. S., Pelfini, M., Zerboni, A. (2023): Estimating the Evolution of a Post-Little Ice Age Deglaciated Alpine Valley through the DEM of Difference (DoD). Remote

Sensing 15(12): 3190, https://doi.org/10.3390/rs15123190.

Benn, D. I., Bolch, T., Hands, K., Gulley, J., Luckman, A., Nicholson, L. I., Quincey, D., Thompson, S., Toumi, R., Wiseman, S. (2012): Response of debris-covered glaciers in the Mount Everest region to recent warming, and implications for outburst flood hazards. Earth-Science Reviews 114, 156–174, https://doi.org/10.1016/j.earscirev.2012.03.008.

Berthier, E., Arnaud, Y., Kumar, R., Ahmad, S., Wagnon, P., Chevallier, P. (2007): Remote sensing estimates of glacier mass balances in the Himachal Pradesh (Western Himalaya, India). Remote Sensing of Environment 108(3), 327–338, https://doi.org/10.1016/J.RSE.2006.11.017.

Berthier, E., Cabot, V., Vincent, C., Six, D. (2016). Decadal region-wide and glacier-wide mass balances derived from multi-temporal aster satellite digital elevation models. Validation over the mont-blanc area. Frontiers in Earth Science 4: 194833, https://doi.org/10.3389/feart.2016.00063.

Bhambri, R., Hewitt, K., Kawishwar, P., Pratap, B. (2017): Surge-type and surge-modified glaciers in the Karakoram. Scientific Reports 7: 15391, https://doi.org/10.1038/s41598-017-15473-8.

Bhambri, R., Schmidt, S., Chand, P., Nüsser, M., Haritashya, U., Sain, K., Tiwari, S. K., Yadav, J. S. (2023): Heterogeneity in glacier thinning and slowdown of ice movement in the Garhwal Himalaya, India. Science of The Total Environment 875: 162625, https://doi.org/10.1016/j.scitotenv.2023.162625.

Bolch, T., Buchroithner, M., Pieczonka, T., Kunert, A. (2008): Planimetric and volumetric glacier changes in the Khumbu Himal, Nepal, since 1962 using Corona, Landsat TM and ASTER data. Journal of Glaciology 54(187), 592–600, https://doi.org/10.3189/002214308786570782.

Bolch, T., Pieczonka, T., Benn, D. I. (2011): Multi-decadal mass loss of glaciers in the Everest area (Nepal Himalaya) derived from stereo imagery. The Cryosphere 5, 349–358, https://doi.org/10.5194/tc-5-349-2011.

Bolch, T., Kulkarni, A. V., Kääb, A., Huggel, C., Paul, F., Cogley, J. G., Frey, H., Kargel, J. S., Fujita, K., Scheel, M., Bajracharya, S. R., Stoffel, M. (2012): The State and Fate of Himalayan Glaciers. Science 336, 310–314, https://doi.org/10.1126/science.1215828.

Brenner, A. C., DiMarzio, J. P., Zwally, H. J. (2007): Precision and accuracy of satellite radar and laser altimeter data over the continental ice sheets, IEEE Transactions on Geoscience and Remote Sensing 45(2), 321–331, https://doi.org/10.1109/TGRS.2006.887172.

Brodský, L., Rusnák, S., Schmidt, S., Vilímek, V., Azzoni, R. S., Nüsser, M., Tronti, G., Kropáček, J., Pandey, A. (2024): Interannual spatio-temporal evolution of the supraglacial lakes on the Belvedere Glacier between 2000 and 2023. AUC Geographica 59(2), 214–228, https://doi.org/10.14712/23361980.2024.24.

Brun, F., Buri, P., Miles, E. S., Wagnon, P., Steiner, J., Berthier, E., Ragettli, S., Kraaijenbrink, P. D. A., Immerzeel, W. W., Pellicciotti, F. (2016): Quantifying volume loss from ice cliffs on debris-covered glaciers using high-resolution terrestrial and aerial photogrammetry. Journal of Glaciology 62, 684–695, https://doi.org/10.1017/jog.2016.54.

Chandrasekharan, A., Ramsankaran, R. (2023): Reconstructing 32 years (1989–2020) of annual glacier surface mass balance in Chandra Basin, Western Himalayas, India. Regional Environmental Change 23: 118, https://doi.org/10.1007/s10113-023-02112-4.

Charalampidis, C., Fischer, A., Kuhn, M., Lambrecht, A., Mayer, C., Thomaidis, K., Weber, M. (2018): Mass-Budget Anomalies and Geometry Signals of Three Austrian Glaciers. Frontiers in Earth Science 6: 218, https://doi.org/10.3389/feart.2018.00218.

Cornes, R., van der Schrier, G., van den Besselaar, E. J. M., Jones, P.D. (2018): An Ensemble Version of the E-OBS Temperature and Precipitation Datasets, Journal of Geophysical Research: Atmospheres 123(17), 9391–9409, https://doi.org/10.1029/2017JD028200.

OpenStreetMap contributors (2017): Available online: https://planet.osm.org, url: https://www.openstreetmap.org (accessed on 10.3.2024).

De Gaetani, C. I., Ioli, F., Pinto, L. (2021): Aerial and UAV Images for Photogrammetric Analysis of Belvedere Glacier Evolution in the Period 1977–2019. Remote Sensing 13: 3787, https://doi.org/10.3390/rs13183787.

Farinotti, D., Immerzeel, W. W., de Kok, R. J., Quincey, D. J., Dehecq, A. (2020): Manifestations and mechanisms of the Karakoram glacier Anomaly. Nature Geoscience 13, 8–16, https://doi.org/10.1038/s41561-019-0513-5.

Fischer, L., Huggel, C., Kääb, A., Haeberli, W. (2013): Slope failures and erosion rates on a glacierized high-mountain face under climatic changes. Earth Surface Processes and Landforms 38(8), 836–846, https://doi.org/10.1002/esp.3355.

Fischer, M., Huss, M., Hoelzle, M. (2015): Surface elevation and mass changes of all Swiss glaciers 1980–2010. The Cryosphere 9(2), 525–540, https://doi.org/10.5194/tc-9-525-2015.

Fleischer, F., Otto, J., Junker, R. R., Hölbling, D. (2021): Evolution of debris cover on glaciers of the Eastern Alps, Austria, between 1996 and 2015. Earth Surface Processes and Landforms 46(9), 1673–1691, https://doi.org/10.1002/esp.5065.

Fugazza, D., Valle, B., Caccianiga, M. S., Gobbi, M., Traversa, G., Tognetti, M., Diolaiuti, G. A., Senese, A. (2023): Glaciological and meteorological investigations of an Alpine debris-covered glacier: the case study of Amola Glacier (Italy). Cold Region Science Technology 216: 104008, https://doi.org/10.1016/j.coldregions.2023.104008.

Fujita, K., Nuimura, T. (2011): Spatially heterogeneous wastage of Himalayan glaciers. Proceedings of the National Academy of Sciences of the United States of America 108(34), 14011–14014, https://doi.org/10.1073/pnas.1106242108.

Fyffe, C. L., Brock, B. W., Kirkbride, M. P., Mair, D. W. F., Arnold, N. S., Smiraglia, C., Diolaiuti, G., Diotri, F. (2019): Do debris-covered glaciers demonstrate distinctive hydrological behaviour compared to clean glaciers? Journal of Hydrology 570, 584–597, https://doi.org/10.1016/j.jhydrol.2018.12.069.

Gardelle, J., Berthier, E., Arnaud, Y., Kääb, A. (2013): Region-wide glacier mass balances over the Pamir-Karakoram-Himalaya during 1999–2011. The Cryosphere 7(4), 1263–1286, https://doi.org/10.5194/tc-7-1263-2013.

Geoportale Piemonte (2014). Available online: http://www.geoportale.piemonte.it (accessed on 15. 1. 2024).

Gulley, J., Benn, D. I. (1997): Structural control of englacial drainage systems in Himalayan debris-covered glaciers. Journal of Glaciology 53(182), 399–412, https://doi.org/10.3189/002214307783258378.

Haubeck, K., Prinz, T. (2013): A UAV-Based Low-Cost Stereo Camera System for Archaeological Surveys – Experiences from Doliche (Turkey), International Archives of the Photogrammetry, Remote Sensing and Spatial Information Sciences XL-1/W2, 195–200, https://doi.org/10.5194/isprsarchives-XL-1-W2-195-2013.

Hewitt, K. (2005): The Karakoram anomaly? Glacier expansion and the "elevation effect", Karakoram Himalaya. Mountain Research and Development 25(4), 332–340, https://doi.org/10.1659/0276-4741(2005)025[0332:TKAGEA]2.0.CO;2.

Hewitt, K. (2014): Glaciers of the Karakoram Himalaya: Glacial Environments, Processes, Hazards and Resources. Advances in Asian Human-Environmental Research. Springer, https://doi.org/10.1007/978-94-007-6311-1.

Hock, R., Rasul, G., Adler, C., Cáceres, B., Gruber, S., Hirabayashi, Y., Jackson, M., Kääb, A., Kang, S., Kutuzov, S., Milner, A., Molau, U., Morin, S., Orlove, B., Steltzer, H. (2019): High Mountain Areas, IPCC Special Report on the Ocean and Cryosphere in a Changing Climate, 131-202, https://www.ipcc.ch/site/assets/uploads/sites/3/2019/11/06_SROCC_Ch02_FINAL.pdf.

Hugonnet, R., McNabb, R., Berthier, E., Menounos, B., Nuth, C., Girod, L., Farinotti, D., Huss, M., Dussaillant, I., Brun, F., Kääb, A. (2021): Accelerated global glacier mass loss in the early twenty-first century. Nature 592, 726–731, https://doi.org/10.1038/s41586-021-03436-z.

Huo, D., Bishop, M. P., Bush, A. B. G. (2021): Understanding Complex Debris-Covered Glaciers: Concepts, Issues, and Research Directions. Frontiers in Earth Science 9: 652279, https://doi.org/10.3389/feart.2021.652279.

Huss, M. (2013): Density assumptions for converting geodetic glacier volume change to mass change. The Cryosphere 7(3), 877–887, https://doi.org/10.5194/tc-7-877-2013.

Huss, M., Bauder, A., Funk, M., Hock, R. (2008): Determination of the seasonal mass balance of four Alpine glaciers since 1865. Journal of Geophysical Research 113(1): F01015, https://doi.org/10.1029/2007jf000803.

Huss, M., Bauder, A. (2009): 20th-century climate change inferred from four long-term point observations of seasonal mass balance. Annals of Glaciology 50(50): 207–214, https://doi.org/10.3189/172756409787769645.

Immerzeel, W., Pellicciotti, F., Bierkens, M. (2013): Rising river flows throughout the twenty-first century in two Himalayan glacierized watersheds. Nature Geoscience 6, 742–745, https://doi.org/10.1038/ngeo1896.

Ioli, F., Bianchi, A., Cina, A., De Michele, C., Maschio, P., Passoni, D., Pinto, L. (2022): Mid-Term Monitoring of Glacier's Variations with UAVs: The Example of the Belvedere Glacier. Remote Sensing 14: 28, https://doi.org/10.3390/rs14010028.

Jóhannesson, T., Raymond, C., Waddington, E. (1989): Time-Scale for Adjustment of Glaciers to Changes in Mass Balance. Journal of Glaciology 35(121), 355–369, https://doi.org/10.3189/S002214300000928X.

Jouvet, G., Huss, M. (2019): Future retreat of Great Aletsch Glacier. Journal of Glaciology 65, 869–872, https://doi.org/10.1017/jog.2019.52.

Kääb, A., Huggel, C., Barbero, S., Chiarle, M. Cordola, M., Epifani, F., Haeberli, W., Mortara, G., Semino, P., Tamburini, A., Viazzo, G. (2004): Glacier hazards at Belvedere Glacier and the Monte Rosa East Face, Italian Alps: Processes and Mitigation. Internationales Symposion Interpraevent 2004 – Riva/Trient. https://www.researchgate.net/publication/242231211_Glacier_hazards_at_Belvedere_glacier_and_the_Monte_Rosa_east_face_Italian_Alps_Processes_and_mitigation.

Kääb, A., Berthier, E., Nuth, C., Gardelle, J., Arnaud, Y. (2012): Contrasting patterns of early twenty-first-century glacier mass change in the Himalayas. Nature 488, 495–498, https://doi.org/10.1038/nature11324.

Kendall, M. G. (1957). Review of Rank Correlation Methods. Biometrika, 44(1/2), 298–298, https://doi.org/10.2307/2333282.

Knuth, F., Shean, D., Bhushan, S., Schwat, E., Alexandrov, O., McNeil, C., Dehecq, A., Florentine, C., O'Neel, S. (2023): Historical Structure from Motion (HSfM): Automated processing of historical aerial photographs for long-term topographic change analysis. Remote Sensing of Environment 285: 113379, https://doi.org/10.1016/j.rse.2022.113379.

Kirkbride, M. P., Deline, P. (2013): The formation of supraglacial debris covers by primary dispersal from transverse englacial debris bands. Earth Surface Processes and Landforms 38(15), 1779–1792, https://doi.org/10.1002/ESP.3416.

Kropáček, J., Mehrishi, P., Bollati, I. M., Brodský, L., Pelfini, M., Azzoni, R., Schmidt, S., Nüsser, M., Vilímek, V. (2024): Dynamics and related natural hazards of Belvedere Glacier in the Italian Alps: a review. AUC Geographica 59(2), 163–183, https://https://doi.org/10.14712/23361980.2024.21.

Laha, S., Kumari, R., Singh, S., Mishra, A., Sharma, T., Banerjee, A., Nainwal, H. C., Shankar, R. (2017). Evaluating the contribution of avalanching to the mass balance of Himalayan glaciers. Annals of Glaciology 58(75pt2), 110–118, https://doi.org/10.1017/aog.2017.27.

Lemke, P., Ren, J., Alley, R. B., Allison, I., Carrasco, J., Flato, G., Fujii, Y., Kaser, G., Mote, P., Thomas, R. H., Zhang, T. (2007): Observations: Changes in Snow, Ice and Frozen Ground. Climate Change: The Physical Science Basis. Contribution of Working Group I to the Fourth Assessment Report of the Intergovernmental Panel on Climate Change [Solomon, S., Qin, D., Manning, M., Chen, Z., Marquis, M., Averyt, K. B., Tignor, M., Miller, H. L. (eds.)]. Cambridge University Press, Cambridge, United Kingdom and New York, NY, USA, https://www.ipcc.ch/site/assets/uploads/2018/02/ar4-wg1-chapter4-1.pdf.

Mattson, L. E., Gardner, J. S., Young, G. J. (1993): Ablation on debris covered glaciers: an example from the Rakhiot Glacier, Punjab, Himalaya. Snow and Glacier Hydrology. IAHS Publication 218, 289–294.

Maurer, J. M., Schaefer, J. M., Rupper, S., Corley, A. (2019): Acceleration of ice loss across the Himalayas over the past 40 years. Science Advances 5(6): eaav7266, https://doi.org/10.1126/sciadv.aav7266.

Mölg, N., Ferguson, J., Bolch, T., Vieli, A. (2020): On the influence of debris cover on glacier morphology: How

high-relief structures evolve from smooth surfaces. Geomorphology 357: 107092, https://doi.org/10.1016/j.geomorph.2020.107092.

Mondino, E. B. (2015): Multi-temporal image co-registration improvement for a better representation and quantification of risky situations: the Belvedere Glacier case study. Geomatatics, Natural Hazards and Risk 6(5–7), 362–378, https://doi.org/10.1080/19475705.2014.927804.

Mortara, G., Tamburini, A., Ercole, G., Semino, P., Chiarle, M., Godone, F., Guiliano, M., Haeberli, W., Kääb, A., Huggel, Ch., Fischer, L., Cordola, M., Barbero, S., Salandin, A., Rabuffetti, D., Mercalli, L., Cat Berro, D., Carton, A., Mazza, A., Godone, D., Federici, P., Viazzo, G., Epifani, F., Valsesia, T. (2009): Il ghiacciaio del Belvedere e l'emergenza del Lago Effimero. Regione Piemonte. Bussoleno: Societa' Meteorologica Subalpina.

Muhammad, S., Tian, L., Ali, S., Latif, Y., Wazir, M. A., Goheer, M. A., Saifullah, M., Hussain, I., Shiyin, L. (2020): Thin debris layers do not enhance melting of the Karakoram glaciers. Science of The Total Environment 746: 141119, https://doi.org/10.1016/J.SCITOTENV.2020.141119.

Nüsser, M., Schmidt, S. (2021): Glacier changes on the Nanga Parbat 1856–2020: A multi-source retrospective analysis. Science of The Total Environment 785: 147321, https://doi.org/10.1016/j.scitotenv.2021.147321.

Nuimura, T., Fujita, K., Yamaguchi, S., Sharma, R. R. (2012): Elevation changes of glaciers revealed by multitemporal digital elevation models calibrated by GPS survey in the Khumbu region, Nepal Himalaya, 1992-2008. Journal of Glaciology 58(210), 648–656, https://doi.org/10.3189/2012JoG11J061.

Nuimura, T., Fujita, K., Sakai, A. (2017). Downwasting of the debris-covered area of Lirung Glacier in Langtang Valley, Nepal Himalaya, from 1974 to 2010. Quaternary International 455, 93–101, https://doi.org/10.1016/J.QUAINT.2017.06.066.

Nuth, C. Kääb, A. (2011): Co-registration and bias corrections of satellite elevation data sets for quantifying glacier thickness change. The Cryosphere 5(1), 271–290, https://doi.org/doi:10.5194/tc-5-271-2011.

Oerlemans, J., Reichert B.K. (2000): Relating glacier mass balance to meteorological data by using a seasonal sensitivity characteristic. Journal of Glaciology 46(152), 1–6, https://doi.org/10.3189/172756500781833269.

Paul, F., Bolch, T., Kääb, A., Nagler, T., Nuth, C., Scharrer, K., Shepherd, A., Strozzi, T., Ticconi, F., Bhambri, R., Berthier, E., Bevan, S., Gourmelen, N., Heid, T., Jeong, S., Kunz, M., Lauknes, T. R., Luckman, A., Merryman Boncori, J. P., Moholdt, G., Muir, A., Neelmeijer, J., Rankl, M., VanLooy, J., Van Niel, T., (2015): The glaciers climate change initiative: Methods for creating glacier area, elevation change and velocity products. Remote Sensing of the Environment 162, 408–426, https://doi.org/10.1016/j.rse.2013.07.043.

Pellicciotti, F., Stephan, C., Miles, E., Herreid, S., Immerzeel, W. W., Bolch, T. (2015): Mass-balance changes of the debris-covered glaciers in the Langtang Himal, Nepal, from 1974 to 1999. Journal of Glaciology 61(226), 373–386, https://doi.org/10.3189/2015JoG13J237.

Pix4D (2024). Pix4Dcapture software available online: https://www.pix4d.com/product/pix4dcapture/ (accessed on 25 January 2024).

Racoviteanu, A. E., Nicholson, L., Glasser, N. F., Miles, E., Harrison, S., Reynolds, J. M. (2022): Debris-covered glacier systems and associated glacial lake outburst flood hazards: challenges and prospects. Journal of the Geological Society 179: jgs2021-084, https://doi.org/10.1144/jgs2021-084.

Radić, V., Hock, R. (2006): Modeling future glacier mass balance and volume changes using ERA-40 reanalysis and climate models: A sensitivity study at Storglaciären, Sweden. Journal of Geophysical Research: Earth Surface 111(F3): 3003, https://doi.org/10.1029/2005JF000440.

Rignot, E., Rivera, A., Casassa, G. (2003): Contribution of the Patagonia Icefields of South America to Sea Level Rise. Science 302(5644), 434–437, https://doi.org/10.1126/science.1087393.

Salerno, F., Thakuri, S., Tartari, G., Nuimura, T., Sunako, S., Sakai, A., Fujita, K. (2017): Debris-covered glacier anomaly? Morphological factors controlling changes in the mass balance, surface area, terminus position, and snow line altitude of Himalayan glaciers. Earth Planetary Science Letters 471, 19–31, https://doi.org/10.1016/j.epsl.2017.04.039.

Scherler, D., Wulf, H., Gorelick, N. (2018): Global Assessment of Supraglacial Debris-Cover Extents. Geophysical Research Letters 45(21), 11798–11805, https://doi.org/10.1029/2018GL080158.

Schmidt, S., Nüsser, M. (2009): Fluctuations of Raikot Glacier during the past 70 years: a case study from the Nanga Parbat massif, northern Pakistan. Journal of Glaciology 55(194), 949–959, https://doi.org/10.3189/002214309790794878.

Smiraglia, C., Azzoni, R. S., D'Agata, C. A. R. L. O., Maragno, D., Fugazza, D., Diolaiuti, G. A. (2015): The evolution of the Italian glaciers from the previous database to the New Italian Inventory. Preliminary considerations and results. Geografia Fisica e Dinamica Quaternaria 38(1), 79–87.

Sommer, C., Malz, P., Seehaus, T. C., Lippl, S., Zemp, M., Braun, M. H. (2020): Rapid glacier retreat and downwasting throughout the European Alps in the early 21st century. Nature Communications 11: 3209, https://doi.org/10.1038/s41467-020-16818-0.

Tamburini, A., Villa, F., Fischer, L., Hungr, O., Chiarle, M., Mortara, G. (2013): Slope Instabilities in High-Mountain Rock Walls. Recent Events on the Monte Rosa East Face (Macugnaga, NW Italy). In: Margottini, C., Canuti, P., Sassa, K. (eds.): Landslide Science and Practice. Springer Berlin Heidelberg, Berlin, Heidelberg, https://doi.org/10.1007/978-3-642-31310-3_44.

Thakuri, S., Salerno, F., Smiraglia, C., Bolch, T., D'Agata, C., Viviano, G., Tartari, G. (2014): Tracing glacier changes since the 1960s on the south slope of Mt. Everest (central Southern Himalaya) using optical satellite imagery. The Cryosphere 8(4), 1297–1315, https://doi.org/10.5194/tc-8-1297-2014.

Tonolo, F. G., Cina, A., Manzino, A., and Fronteddu, M. (2020): 3D Glacier Mapping by Means of Satellite Stereo Images: The Belvedere Glacier Case Study in the Italian Alps. The International Archives of the Photogrammetry, Remote Sensing and Spatial Information Sciences, XLIII-B2-2020, 1073–1079, https://doi.org/10.5194/isprs-archives-XLIII-B2-2020-1073-2020.

Truffer, M., Kääb, A., Harrison, W. D., Osipova, G. B., Nosenko, G. A., Espizua, L., Gilbert, A., Fischer, L., Huggel, C., Craw

Burns, P. A., Lai, A. W. (2021): Glacier surges, in: Snow and Ice-Related Hazards, Risks, and Disasters. Elsevier, 417–466, https://doi.org/10.1016/B978-0-12-817129-5.00003-2.

Westoby, M. J., Rounce, D. R., Shaw, T. E., Fyffe, C. L., Moore, P. L., Stewart, R. L., Brock, B. W. (2020): Geomorphological evolution of a debris-covered glacier surface. Earth Surface Processes and Landforms 45(14), 3431–3448, https://doi.org/10.1002/esp.4973.

Yao, T., Thompson, L., Yang, W., Yu, W., Gao, Y, Guo, X., Yang, X, Duan, K., Zhao, H., Xu, B., Pu, J., Lu, A., Xiang, Y., Kattel, D. B., Joswiak, D. (2012): Different glacier status with atmospheric circulations in Tibetan Plateau and surroundings. Nature Climate Change 2, 663–667, https://doi.org/10.1038/nclimate1580.

Zemp, M., Huss, M., Thibert, E., Eckert, N., McNabb, R., Huber, J., Barandun, M., Machguth, H., Nussbaumer, S. U., Gärtner-Roer, I., Thomson, L., Paul, F., Maussion, F., Kutuzov, S., Cogley, J. G. (2019): Global glacier mass changes and their contributions to sea-level rise from 1961 to 2016. Nature 568, 382–386, https://doi.org/10.1038/s41586-019-1071-0.

Zeileis, A., Leisch, F., Hornik, K., and Kleiber, C. (2002). Strucchange: An R package for testing for structural change in linear regression models. Journal of Statistical Software 7(2), 1–38, https://doi.org/10.18637/jss.v007.i02.

Zemp, M., Hoelzle, M., Haeberli, W. (2009): Six decades of glacier mass-balance observations: a review of the worldwide monitoring network. Annals of Glaciology 50(50), 101–111, https://doi.org/10.3189/172756409787769591.

WGMS (2024): Fluctuations of Glaciers Database. World Glacier Monitoring Service (WGMS), Zurich, Switzerland, https://doi.org/10.5904/wgms-fog-2024-01.

Appendix

This supplement offers a supplementary analysis of temperature time series data (Appendix 1) for the location of Belvedere Glacier. The supplementary data and analysis facilitate comprehension of the long-term trends pertinent to the article's primary focus: the intricate, spatially heterogeneous patterns of glacier elevation change resulting from debris cover, avalanches, surge-type events, supraglacial meltwater, and glacial lake outburst floods in the context of global warming.

The data were obtained from the E-OBS dataset, which was generated as part of the EU-FP6 UERRA project (http://www.uerra.eu), and from the Copernicus Climate Change Service. The initial 0.1-degree grid data for daily mean temperature were aggregated to yield annual mean temperature data. A Mann-Kendall test (Kendall 1957) was conducted to identify any potential trends in temperature. The test yielded a p-value of 5.75×10^{-14}, indicating a statistically significant increasing trend. Furthermore, the break dates algorithm, as developed by Zeileis et al. (2002), was used. The analysis identified a breakpoint in 1987 based on the annual mean temperature time series.
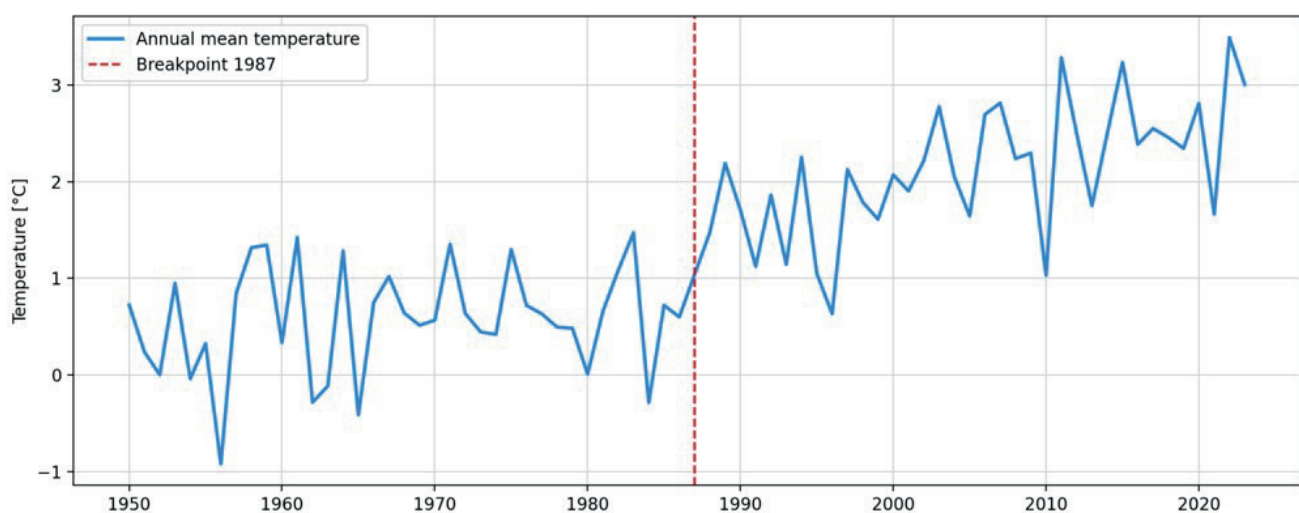
Appendix 1 Annual mean temperature time-series for Belvedere Glacier with breakpoint analysis.